Structural Engineering and Mechanics, *Vol. 53, No. 4 (2015) 745-765*
DOI: http://dx.doi.org/10.12989/sem.2015.53.4.745

Nonlinear numerical simulation of RC columns subjected to cyclic oriented lateral force and axial loading

Kabir Sadeghi*

Civil Engineering Department, Girne American University, Karmi Campus, Girne, KKTC, via Mersin 10, Turkey

(Received August 8, 2014, Revised December 12, 2014, Accepted December 16, 2014)

Abstract. A nonlinear Finite Element (FE) algorithm is proposed to analyze the Reinforced Concrete (RC) columns subjected to Cyclic Loading (CL), Cyclic Oriented Lateral Force and Axial Loading (COLFAL), Monotonic Loading (ML) or Oriented Pushover Force and Axial Loading (OPFAL) in any direction. In the proposed algorithm, the following parameters are considered: uniaxial behavior of concrete and steel elements, the pseudo-plastic hinge produced in the critical sections, and global behavior of RC columns. In the proposed numerical simulation, the column is discretized into two Macro-Elements (ME) located between the pseudo-plastic hinges at critical sections and the inflection point. The critical sections are discretized into Fixed Rectangular Finite Elements (FRFE) in general cases of CL, COLFAL or ML and are discretized into Variable Oblique Finite Elements (VOFE) in the particular cases of ML or OPFAL. For pushover particular case, a fairly fast converging and properly accurate nonlinear simulation method is proposed to assess the behavior of RC columns. The proposed algorithm has been validated by the results of tests carried out on full-scale RC columns.

Keywords: Numerical simulation; reinforced concrete; columns; cyclic or monotonic loading

1. Introduction

In recent years, increased demand for using performance based design methods have made researchers intensify their efforts to modify and enhance the accuracy of nonlinear static procedures on a variety of structural models. A number of those methods have been implemented in different design codes and guidelines. These procedures apply constant load patterns such as equivalent lateral force, first mode shape and response combination load patterns in performing pushover analyses (Rofooei *et al*. 2011).

A range of approaches has been used to analyze the behavior of RC sections under biaxial bending moment and axial loading (BBMAL). The simplified models of the earlier approaches do not reflect the nonlinearity of materials. Richard Yen (1991) has proposed a model to calculate RC sections under biaxial bending moment (BBM) based on the position of the neutral axis and the percentage of longitudinal reinforcement. In this method, many simplifications are used that have a detrimental effect on the precision of the results. Yau *et al*. (1993) have proposed a method to calculate the ultimate strength of the sections under BBM using the percentage of longitudinal

*Corresponding author, Associate Professor, E-mail: ksadeghi@gau.edu.tr, kabirsadeghi@gmail.com

http://www.techno-press.org/?journal=sem&subpage=8 ISSN: 1225-4568 (Print), 1598-6217 (Online)

reinforcement and the distance between the neutral axis and the point with maximum compressive stress, as main parameters. Alnoury and Chen (1982) have proposed a method using the tangent of the force-displacement curve and the local rigidity in the section level. The model proposed by Hsu and Mirza (1973), which uses the developed Newton-Raphson method and simplified models of strain-stress curves for concrete and reinforcement, is not applicable for the descending branch of the moment-curvature (M-ϕ) curve. Brondum-Nielsen (1984) has proposed a method to calculate the ultimate strength of the sections under BBM using the developed Newton-Raphson method and simplified rectangular model of strain-stress for concrete recommended by CEB-FIP code. Zak (1993) has also proposed a method to calculate the ultimate strength of the sections under BBM using the developed Newton-Raphson method. The Newton-Raphson method yields a fast solution, but presents problems while passing the peak point of the response curve and near the inflection point that causes divergence of the solution. Newton's method is well adapted for monotonic curves and needs to be transformed at each relative extreme point occurrence. The maxima have to be evaluated anyway. The Ricks method is derived from Newton’s and allows the user to cross over the peaks. Newton and Ricks processes must be used with caution in numerical simulation.

Some methods such as those proposed by Amziane and Dubé (2008) are applicable to RC structures under uniaxial cyclic bending with axial load. Massumi and Monavari (2013) have proposed an energy-based method to obtain the target displacement for reinforced concrete frames under cyclic loading assuming that the capacity energy absorption of the structures for both the pushover and cyclic analyses are equal. Dundar and Tokgoz (2012) tested, experimentally, the strength of biaxially loaded short and slender RC columns of square and L-shaped sections with high strength concrete and compared with a theoretical method based on the fiber element technique.

Different building codes, based on their local conditions, consider different assumptions, methods and criteria to design RC members and give different results. As an example, Tabsh (2013) shows that the differences between the design capacities in the ACI 318 and BS 8110 codes are minor for flexure, moderate for axial compression, and major for shear.

Among several existing techniques, used to analyze RC sections under BBMAL, two are the most common: direct search procedures to determine either the strain equilibrium plane or the location of the neutral axis.

Except for the case of the linear approach where exact integration rules can be used, the section can be discretized into parallel layers rotating parallel to the neutral axis. This method can be applied only in the ML case. Another approach is to discretize the cross-section into FRFE. This method can be used under any CL or ML cases.

The aim of this paper is to present a numerical simulation algorithm to assess the behavior of RC columns under COLFAL or OPFAL in any direction (i.e., sections under BBMAL). This is achieved by using FRFE or VOFE in the discretization of the sections based on the local degradation of materials.

2. Proposed numerical simulation approach

2.1 Description of the proposed algorithm

In the proposed simulation algorithm, the column is decomposed into two ME positioned between the inflection point (zero moment) and critical sections (maxim moments). Then the nonlinear behavior of ME are analyzed. In fact a Macro-Element acts as fixed bottom-free top half-columns under biaxial cyclic bending moment (i.e., lateral force in any direction) with axial load. Finally, the two connected ME are assembled to determine the global behavior of the column.

To find the status of the entire column, the applied loads and also the secondary moments, due to P-Δ effect, are considered in the simulation of the column.

In the proposed algorithm, for each concrete and reinforcement element a uniaxial behavior is considered and their strain distributions are assumed to form a plane which remains a plane during deformation (Kinematics Navier's hypothesis). The stresses of concrete and steel are expressed as nonlinear functions of strains (ε) in each (i, j) concrete and (k) steel elements (see Fig. 1). For compressive confined and unconfined concrete elements the cyclic stress-strain model proposed by Sadeghi (1995, 2001, 2014) and for reinforcements, the expression proposed by Park and Kent (1972) based on the Ramberg-Osgood cyclic model have been used in the proposed simulation algorithm. The concrete tensile stress is assumed to be linear up to the concrete tensile strength. To determine the maximum compression strain value (ε_{CU}) of unconfined concrete, Eq. (1) given by CEB Code (1978) has been used. This equation is particularly applicable where there is a loss of concrete cover outside the stirrups

$$\varepsilon_{CU} = (4 - 0.02f_c')/1000 \qquad (f_c' \text{ in MPa}) \qquad (1)$$

where f_c'represents 28-days compressive strength of unconfined concrete.

To determine the failure of confined concrete in the proposed simulation, Eq. (2) proposed by Sheikh (1982) has been used

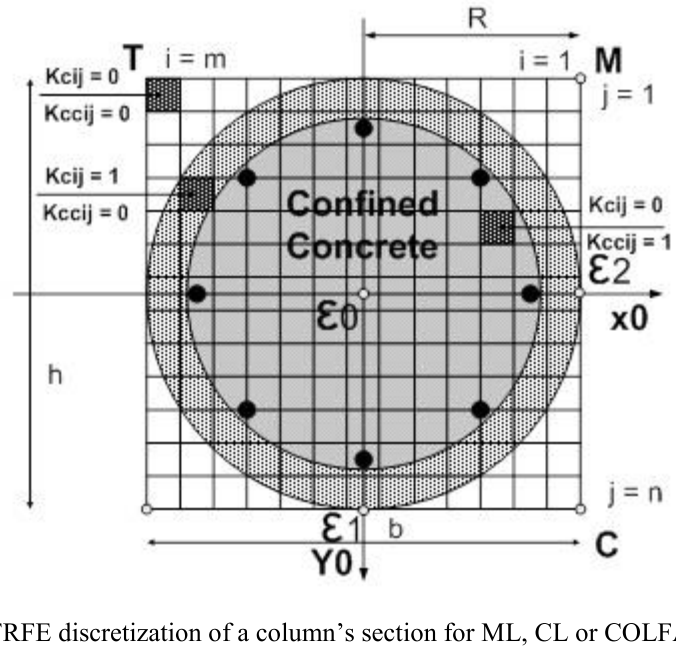

Fig. 1 FRFE discretization of a column's section for ML, CL or COLFAL cases

$$\varepsilon_{CCU} = 0.004 + (0.9\rho_s . f_{yh})/300 \qquad (f_{yh} \text{ in MPa}) \tag{2}$$

where ε_{CCU} presents the maximum compression strain value of confined concrete, ρ_s represents the ratio of transversal reinforcement volume per concrete volume situated inside the stirrups and f_{yh} represents the yielding stress of the stirrups.

The basic equilibrium is justified over a critical hypothetical cross-section assuming the Navier law with an average curvature. The method used qualifies as a “Strain Plane Control Process” that requires the resolution of a quasi-static simultaneous equations system using a triple iteration process over the strains when the FRFE option (Sadeghi 2011) is applied and an iteration process to find the neutral axis position when the VOFE option is applied. The calculations are based on the cyclic non-linear stress-strain relationships for concrete and reinforcement FE. In order to reach equilibrium, when the FRFE option is applied, three main strain parameters ε_C (the strains in the extreme compressive point), ε_T (the strains in the extreme tensile point) and ε_M (the strain in the point *M* located at another corner of the section) are used as three main variables as shown in Fig. 1. For non-rectangular sections these points *C*, *T* and *M* may be outside the actual cross-sections and be located on the discretizing mesh frontiers).

2.2 Discretization principles

2.2.1 Discretization principles when CL or COLFAL is applied (general case)

The critical sections are discretized into FRFE in general cases of CL or COLFAL and in VOFE in particular cases of ML or OPFAL. Since to follow up on the loading-unloading path, each of the last three loading-unloading steps should be saved, the FRFE discretization type that the positions of the centers of gravity of FRFE are fixed have been applied.

2.2.2 Discretization principles when ML or OPFAL is applied (particular case)

In the pushover (monotonic) loading cases, the sections of the column are discretized into VOFE that always stay parallel to the neutral axis. Two different widths are adopted for VOFE in a section. The frontier between two zones A and B which can have different oblique element widths are selected to pass a fixed point M at the corner of a section as shown in Fig. 2. In this case, the number of elements is limited to “*m*+*n*”, while if using FRFE discretization, the section is discretized into “*m*.*n*” elements (m and n are numbers of elements along the smaller and larger sides of the section, respectively).

Since, zone A is usually under tension or under low compression stresses and its contribution in resisting axial force and bending moments is low, the width of elements situated in zone A can be selected to be greater than the width of elements situated in zone B. This reduces the number of elements. By using this VOFE discretization type, the time of calculation is significantly slightly decreased and since the proposed oblique elements always stay parallel to the neutral axis, there is a uniform stress distribution along each oblique element, which increases the accuracy of the results. The results obtained from the proposed numerical simulations illustrate that, when the same values for the widths of VOFE and FRFE are applied (in orders magnitude of 1 to 2 cm), the time of calculation is about 10% lesser for the case of using VOFE.

In this discretization method, the inclinations of the oblique finite elements and the position of their respective centers of gravity are variable. To calculate columns under ML or OPFAL, there is no need to save the obtained results of the previous steps of loading, which significantly slightly saves the calculation time.

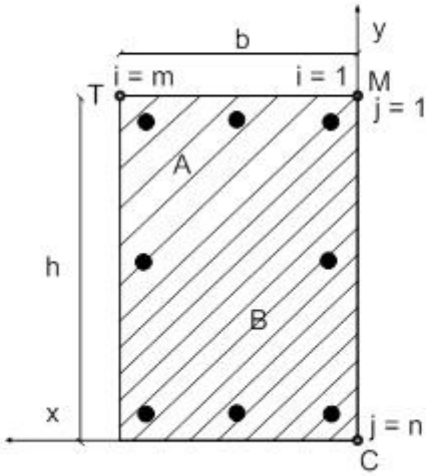

Fig. 2 Discretization of a section into VOFE for ML or OPFAL cases

2.3 Equilibrium conditions

2.3.1 Quasi-static equilibrium of the section

The fundamental relationships determining the equilibrium state of the sections are as follows:

a) - Equilibrium equation of axial forces in the center of the column section,

b) - Equilibrium equations of bending moments at the column section.

The general equilibrium system of each section consists of three nonlinear relations equating external and internal effects

$$N_{ext} = N_{int} \tag{3}$$

$$Mx_{ext} = Mx_{int} \tag{4}$$

$$My_{ext} = My_{int} \tag{5}$$

where

$$M_{ext} = [(Mx_{ext})^2 + (My_{ext})^2]^{1/2} \tag{6}$$

$$M_{int} = [(Mx_{int})^2 + (My_{int})^2]^{1/2} \tag{7}$$

where N_{ext} and N_{int} represent the external and internal axial forces, respectively; Mx_{ext}, My_{ext}, Mx_{int} and My_{int} represent the external and internal bending moments about the orthogonal x_0 and y_0 axes passing through the centroid of the cross-section, respectively (see Figs. 1 and 3); M_{ext} and M_{int} represent the total external and internal bending moments. Mx_{int} and My_{int} are defined in Sections 2.3.2 and 2.3.3 below.

The proposed method requires the resolution of a quasi-static simultaneous equations system using a triple iteration process over the strains which depends on the position of the neutral axis. It is based also on the nonlinear stress-strain relationships for concrete and reinforcement FE.

2.3.2 Quasi-static equilibrium of the section for CL or COLFAL cases (general case)

For the CL or COLFAL case, the internal efforts are as follows

$$N_{int} = \sum_i^m \sum_j^n Kcc_{ij} . \sigma cc_{ij} . A_{ij} + \sum_i^m \sum_j^n Kc_{ij} . \sigma c_{ij} . A_{ij} + \sum_k^{ns} \sigma s_k . As_k \tag{8}$$

$$Mx_{int} = \sum_i^m \sum_j^n Kcc_{ij} . \sigma cc_{ij} . y_{ij} . A_{ij} + \sum_i^m \sum_j^n Kc_{ij} . \sigma c_{ij} . y_{ij} . A_{ij} + \sum_k^{ns} \sigma s_k . y_k . As_k \tag{9}$$

$$My_{int} = \sum_i^m \sum_j^n Kcc_{ij} . \sigma cc_{ij} . x_{ij} . A_{ij} + \sum_i^m \sum_j^n Kc_{ij} . \sigma c_{ij} . x_{ij} . A_{ij} + \sum_k^{ns} \sigma s_k . x_k . As_k \tag{10}$$

where σcc_{ij}, σc_{ij} and σs_k represent the stresses of confined concrete, unconfined concrete and steel FE, respectively; A_{ij} and As_k are the concrete and steel element areas. The Kcc_{ij} and Kc_{ij} factors are used to indicate whether the (i, j) element belongs to the confined concrete, unconfined concrete or an imaginary part of the section and also show the status of concrete cover. Kcc_{ij}=1, for a confined concrete element and Kc_{ij}=1, for an unconfined concrete element. Kccij=0 and Kcij=0 for the other imaginary elements in the case of nonrectangular section, or for the elements when fail; ns is the total number of longitudinal reinforcement in the section; $m=i_{\max}$ and $n=j_{\max}$. For a nonrectangular section, a virtual rectangular grid section is used (Sadeghi 1995) (see Fig. 1).

For this case, to reach equilibrium, three main characteristic parameters ε_C, ε_T and ε_M are used as the three main unknown variables.

2.3.3 Quasi-static equilibrium of the section for ML or OPAL cases (particular case)

For the ML or OPFAL case, the internal efforts are as follows

$$N_{int} = \sum_i^m \sigma_i A_i + \sum_j^n \sigma_j A_j + \sum_k^{ns} \sigma s_k \, As_k \tag{11}$$

$$Mx_{int} = \sum_i^m \sigma_i A_i \, y_i + \sum_j^n \sigma_j A_j \, y_j + \sum_k^{ns} \sigma s_k \, As_k y_k \tag{12}$$

$$My_{int} = \sum_i^m \sigma_i A_i \, x_i + \sum_j^n \sigma_j A_j \, x_j + \sum_k^{ns} \sigma s_k \, As_k x_k \tag{13}$$

where σ_i and σ_j represent the equivalent stresses considering confined and unconfined concretes contributions in FE numbers i and j, respectively; A_i, A_j and As_k are the areas of concrete element i (at zone A), concrete element j (at zone B) and steel elements, respectively (see Fig. 2).

For this case, to reach equilibrium, three main characteristic parameters ε_C, X_n and Y_n are used as the three main unknown variables. Where Xn and Yn represent the coordinates of two points E and F at the intersections of the neutral axis with X and Y axes located on two perpendicular edges of the section, as shown in Fig. 3.

2.4 Determination of strains

2.4.1 Determination of strains (general case)

The strains in the concrete and steel FE are calculated by applying the following equations

$$\varepsilon_{ij} = \varepsilon_0 + \phi_x (x_{ij} - x_0) + \phi_y (y_{ij} - y_0) \tag{14}$$

$$\varepsilon s_k = \varepsilon_0 + \phi_x (xs_k - x_0) + \phi_y (ys_k - y_0) \tag{15}$$

with

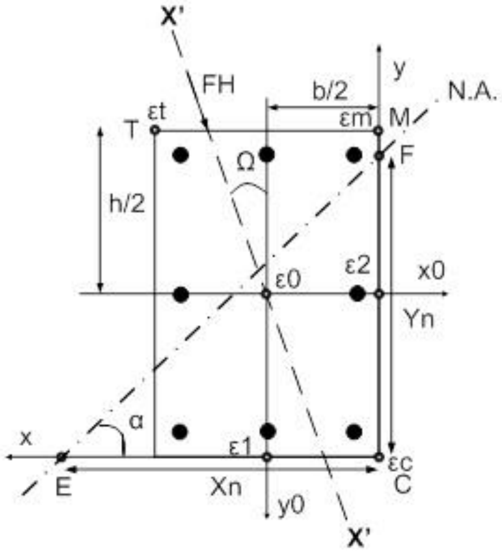

Fig. 3 Position of neutral axis and characteristic strains on a section for ML or OPFAL cases

$$\varepsilon_0 = \frac{\varepsilon_C + \varepsilon_T}{2} \tag{16}$$

where, ε_0 represents the strain of the section's centroid with coordinates of (x_0, y_0); ϕ_x and ϕ_y are the curvatures in the two main axes of section (see Section 2.5).

2.4.2 Determination of strains (particular case)

The strain values of the concrete and steel FE are determined by taking into consideration the Kinematics Navier's hypothesis. Eq. (17) is established for the strain plane based on strains of three nonaligned characteristic points on the section: *C*, the point representing maximum compression stress, and two points *E* and *F* at the intersections of the neutral axis with *X* and *Y* axes. The origin of *XY* Cartesian coordinates system is located on point *C* (see Fig. 3).

$$\varepsilon = \varepsilon_c \left(1 - \frac{x}{X_n} - \frac{y}{Y_n}\right) \tag{17}$$

where *x* and *y* represent the coordinates of any point on the strain plane and ε represents its strain; ε_c represents the strain at point *C*; X_n and Y_n represent coordinates of points E and F, respectively.

2.5 Determination of curvatures

The curvatures in directions x and y are calculated as follows

$$\phi_x = \frac{(\varepsilon_2 - \varepsilon_0)}{(b/2)} \tag{18}$$

$$\phi_y = \frac{(\varepsilon_1 - \varepsilon_0)}{(h/2)} \tag{19}$$

with

$$\varepsilon_2 = \frac{\varepsilon_C + \varepsilon_M}{2} \tag{20}$$

$$\varepsilon_1 = \varepsilon_C + \frac{\varepsilon_T}{2} - \frac{\varepsilon_M}{2} \tag{21}$$

where *b* and *h* are the smaller and larger dimensions of the section, respectively.

The maximum curvature is given as

$$\phi = \frac{\varepsilon_C}{h'} \tag{22}$$

where h' represents the distance between extreme compression point *C* and neutral axis.

It can be proved that this maximum curvature can be also presented as

$$\phi = \sqrt{{\phi_x}^2 + {\phi_y}^2} \tag{23}$$

In particular cases of ML or OPFAL, the strains at points 0, 1 and 2 (ε_0, ε_1 andε_2) on the section, shown in Figs. 1 and 3, are calculated by applying ε_C, and X_n and Y_n in Eq. (17).

2.6 Determination of neutral axis position

2.6.1 Determination of neutral axis position (general case)

The coordinates of neutral axis intersections with x_0 and y_0 axes are found from Eqs. (24) and (25)

$$x_n = \frac{b}{2} + \left(\frac{h}{2}\right)\left(\frac{\phi_y}{\phi_x}\right) - \frac{\varepsilon_C}{\phi_x} \tag{24}$$

$$y_n = \frac{h}{2} + \left(\frac{b}{2}\right)\left(\frac{\phi_x}{\phi_y}\right) - \frac{\varepsilon_C}{\phi_y} \tag{25}$$

2.6.2 Determination of neutral axis position (particular case)

To find the solution of the equilibrium Eqs. (3), (4) and (5), four cases of movements for each position of neutral axis, composed of two cases of displacement and two cases of rotation are considered (see Fig. 4). For two cases of displacements, two sets of increments of (+Δ*x*, +Δ*y*) and (-Δ*x*, -Δ*y*) are applied, and for two cases of rotations, two sets of increments of (+Δ*x*, -Δ*y*) and (-Δ*x*, +Δ*y*) are applied. Depending on the loading condition, some percentages of dimensions of the section are considered for the values of Δ*x* and Δ*y*. For the low values of axial or lateral loading, the values of Δ*x* and Δ*y* may be chosen relatively bigger values. Based on these four movements and by applying a comparative step-by-step method during the successive steps, the solution for the equilibrium state of forces and bending moments are found. To complete these steps, the differences between external and internal forces and also the differences between external and internal bending moments are reduced to satisfy the acceptable criteria given in Section 2.11. The minimum differences allow one to determine the position of the neutral axis. To find the minimum differences, a linear combination of the resultant bending moment and the axial force normalized to their maximal values are used.

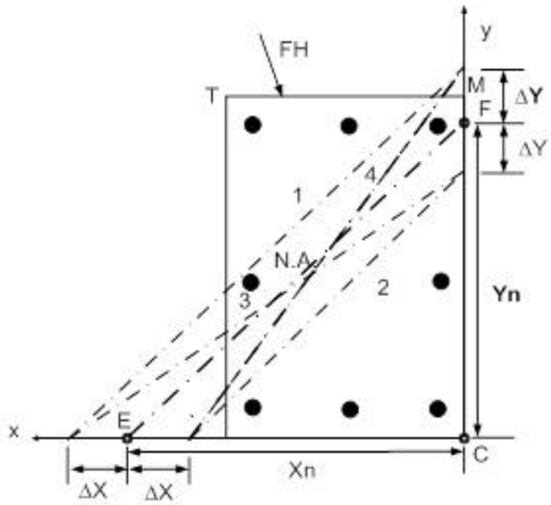

Fig. 4 Four cases depicting increments of neutral axis position for ML or OPFAL cases

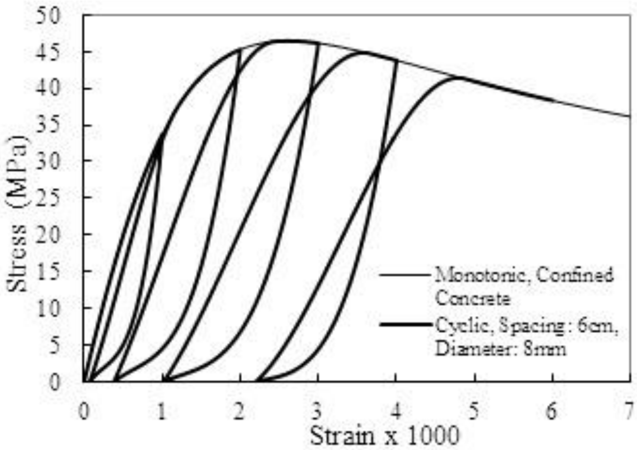

Fig. 5 An example of loading-unloading path for confined concrete FE

2.7 Loading and stress-strain histories

The loading history of concrete and steel FE on the stress-strain curves are saved and compared. This is not only related to the loading history, but also to the position of the FE on the sections. Each step of loading of ME, concrete FE and steel FE are saved to compare with the two previous steps. Two examples of loading-unloading path for confined concrete FE and steel FE are shown in Figs. 5 and 6.

2.7.1 Loading history on sections and ME

Based on the applied external moment or applied relative curvature on the section l for loading step k "$M_{ext}(k,l)$ or $\phi(k,l)$", the parameters "$dM_1$and dM_2", or "$d\phi_1$ and $d\phi_2$" are defined as follows:

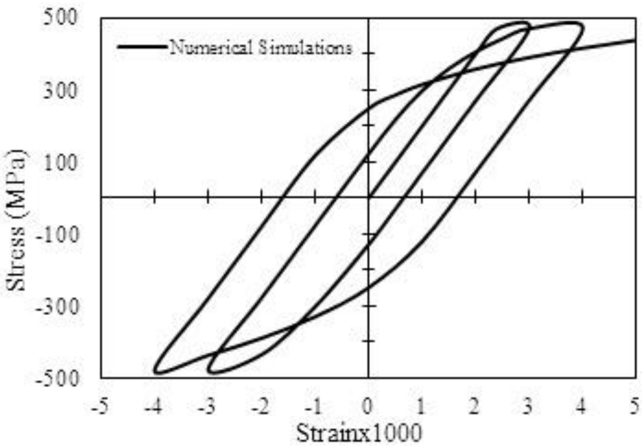

Fig. 6 An example of loading-unloading path for steel FE

For the imposed force case

$$dM_1 = M_{ext}(k-1,l) - M_{ext}(k-2,l) \tag{26}$$

$$dM_2 = M_{ext}(k,l) - M_{ext}(k-1,l) \tag{27}$$

For the imposed curvature (or imposed displacement) case

$$d\phi_1 = \phi(k-1,l) - \phi(k-2,l) \tag{28}$$

$$d\phi_2 = \phi(k-1,l) - \phi(k-2,l) \tag{29}$$

These parameters allow following up the different phases of loading history on the sections. The four different typical trajectories are as follows:

Phase 1 – Loading:

For the imposed force case

$$[dM_1 \geq 0 \text{ and } dM_2 > 0] \tag{30}$$

For the imposed curvature (or imposed displacement) case

$$[d\phi_1 \geq 0 \text{ and } d\phi_2 > 0] \tag{31}$$

Phase 2 – Unloading after loading:

For the imposed force case

$$[dM_1 \geq 0 \text{ and } dM_2 < 0] \tag{32}$$

For the imposed curvature (or imposed displacement) case

$$[d\phi_1 \geq 0 \text{ and } d\phi_2 < 0] \tag{33}$$

Phase 3 – Unloading:

For the imposed force case

$$[dM_1 < 0 \text{ and } dM_2 < 0] \tag{34}$$

For the imposed curvature (or imposed displacement) case

$$[d\phi_1 < 0 \text{ and } d\phi_2 < 0] \tag{35}$$

Phase 4 – Reloading after unloading:
For the imposed force case:

$$[dM_1 < 0 \text{ and } dM_2 > 0] \tag{36}$$

For the imposed curvature (or imposed displacement) case:

$$[d\phi_1 < 0 \text{ and } d\phi_2 > 0] \tag{37}$$

2.7.2 Loading history of concrete and steel FE

Each concrete or steel FE has its own proper loading history, for example, on a section; some FE may be under loading, and in the same time some other FE may be under unloading or reloading phase.

Based on strain of finite element ij of section l for the step k of the loading "$\varepsilon(k,l,i,j)$", the parameters of $d\varepsilon_1$ and $d\varepsilon_2$ are defined as follows

$$d\varepsilon_1 = \varepsilon(k-1,l,i,j) - \varepsilon(k-2,l,i,j) \tag{38}$$

$$d\varepsilon_2 = \varepsilon(k,l,i,j) - \varepsilon(k-1,l,i,j) \tag{39}$$

These parameters allow fixing the limits given for iteration process to research the equilibrium parameters. The four different typical phases are as follows:

Loading phase

$$[d\varepsilon_1 \geq 0 \text{ and } d\varepsilon_2 > 0] \tag{40}$$

Unloading after loading phase

$$[d\varepsilon_1 \geq 0 \text{ and } d\varepsilon_2 < 0] \tag{41}$$

Unloading phase

$$[d\varepsilon_1 < 0 \text{ and } d\varepsilon_2 < 0] \tag{42}$$

Reloading after unloading phase

$$[d\varepsilon_1 < 0 \text{ and } d\varepsilon_2 > 0] \tag{43}$$

The same procedure is used for loading history of steel FE.

2.8 Determination of the equilibrium parameters limits (general case)

In each step of loading for a fixed value of ε_C, the value of ε_T is situated between ε_{Tmin} and ε_{Tmax}, while ε_M is always between ε_C and ε_T.

$$\varepsilon_{Tmin} \leq \varepsilon_T \leq \varepsilon_{Tmax} \tag{44}$$

$$\varepsilon_{Cmin} \leq \varepsilon_C \leq \varepsilon_{Cmax} \tag{45}$$

In loading or reloading cases

$$\varepsilon_T \leq \varepsilon_M \leq \varepsilon_C \tag{46}$$

In unloading cases

$$\varepsilon_T \geq \varepsilon_M \geq \varepsilon_C \tag{47}$$

The determination of these terminal iterations is performed based on the loading history in the following manner:

For the initial loading

$$\varepsilon_{Cmax} = +0.003 \tag{48}$$

$$\varepsilon_{Cmin} = -0.020 \tag{49}$$

$$\varepsilon_{Tmax} = +0.003 \tag{50}$$

$$\varepsilon_{Tmin} = -0.020 \tag{51}$$

For the loading or reloading cases

$$\varepsilon_{Cmax} = +0.003 \tag{52}$$

$$\varepsilon_{Cmin} = -0.050 \text{ or } \varepsilon_C(k-1) \tag{53}$$

$$\varepsilon_{Tmax} = +0.030 \text{ or } \varepsilon_T(k-1) \tag{54}$$

$$\varepsilon_{Tmin} = -0.050 \tag{55}$$

For the unloading cases

$$\varepsilon_{Cmax} = +0.003 \text{ or } \varepsilon_C(k-1) \tag{56}$$

$$\varepsilon_{Cmin} = -0.050 \tag{57}$$

$$\varepsilon_{Tmax} = +0.030 \tag{58}$$

$$\varepsilon_{Tmin} = -0.050 \text{ or } \varepsilon_T(k-1) \tag{59}$$

2.9 Determination of the equilibrium parameters (ε_C, ε_T and ε_M) (general case)

For the strain in the extreme compression point of the section

$$\varepsilon_C = (\varepsilon_{Cmin} + \varepsilon_{Cmax})/2 \tag{60}$$

For the strain in the extreme tension point of the section

$$\varepsilon_T = (\varepsilon_{Tmin} + \varepsilon_{Tmax})/2 \tag{61}$$

For the strain in point *M*

$$\varepsilon_M = (\varepsilon_{Mmin} + \varepsilon_{Mmax})/2 \tag{62}$$

The initial values for ε_{Mmin} and ε_{Mmax} can be considered as ε_T and ε_C, respectively.

2.10 Verification of the equilibrium between the external and internal efforts

2.10.1 Equilibrium between the external and internal orientation angles

The equilibrium between the imposed external and internal orientation angles is verified by performing an iteration process over the strains of point *M* on the section (ε_M) for the given values of ε_C and ε_T as follows (see the flow chart shown in Fig. 7)

$$\varepsilon_{Mmax} = \varepsilon_M \qquad \text{(for } \Omega_{int} > \Omega_{ext}) \tag{63}$$

$$\varepsilon_{Mmin} = \varepsilon_M \qquad \text{(for } \Omega_{int} < \Omega_{ext}) \tag{64}$$

In the next iteration (i+1)th, the following equation is applied:

$$\varepsilon_{M(i+1)} = (\varepsilon_{Mmin(i)} + \varepsilon_{Mmax(i)})/2 \tag{65}$$

By calculating the strains and stresses of concrete and steel FE, internal moments and orientation angles, and verification of the equilibrium of external and internal efforts during a set of the successive iteration process, this should conform to the following equilibrium condition

$$\Omega_{ext} = \Omega_{int} \tag{66}$$

where

$$\Omega_{ext} = \Omega = Tan^{-1}\,(My_{ext}/Mx_{ext}) \tag{67}$$

$$\Omega_{int} = Tan^{-1}\,(My_{int}/Mx_{int}) \tag{68}$$

2.10.2 Equilibrium between the external and internal axial forces

The equilibrium between the imposed external and internal axial forces is verified by performing an iteration process over the strains of extreme tension point *T* on the section (ε_T) for the given value of ε_C as follows (see the flow chart shown in Fig. 7)

$$\varepsilon_{Tmax} = \varepsilon_T \qquad \text{(for } N_{int} > N_{ext}) \tag{69}$$

$$\varepsilon_{Tmin} = \varepsilon_T \qquad \text{(for } N_{int} < N_{ext}) \tag{70}$$

In the next iteration (i+1)th, the following equation is applied

$$\varepsilon_{T(i+1)} = (\varepsilon_{Tmin(i)} + \varepsilon_{Tmax(i)})/2 \tag{71}$$

By calculating the strains and stresses of concrete and steel FE, internal moments and orientation angles and axial forces, and verification of the equilibrium of external and internal efforts during a set of the successive iteration process, this should conform to the following equilibrium condition

$$N_{ext} = N_{int} \tag{72}$$

2.10.3 Equilibrium between the external and internal moments

The equilibrium between the imposed external and internal moments is verified by performing an iteration process over the strains of extreme compression point *C* as follows (see the flow chart shown in Fig. 7)

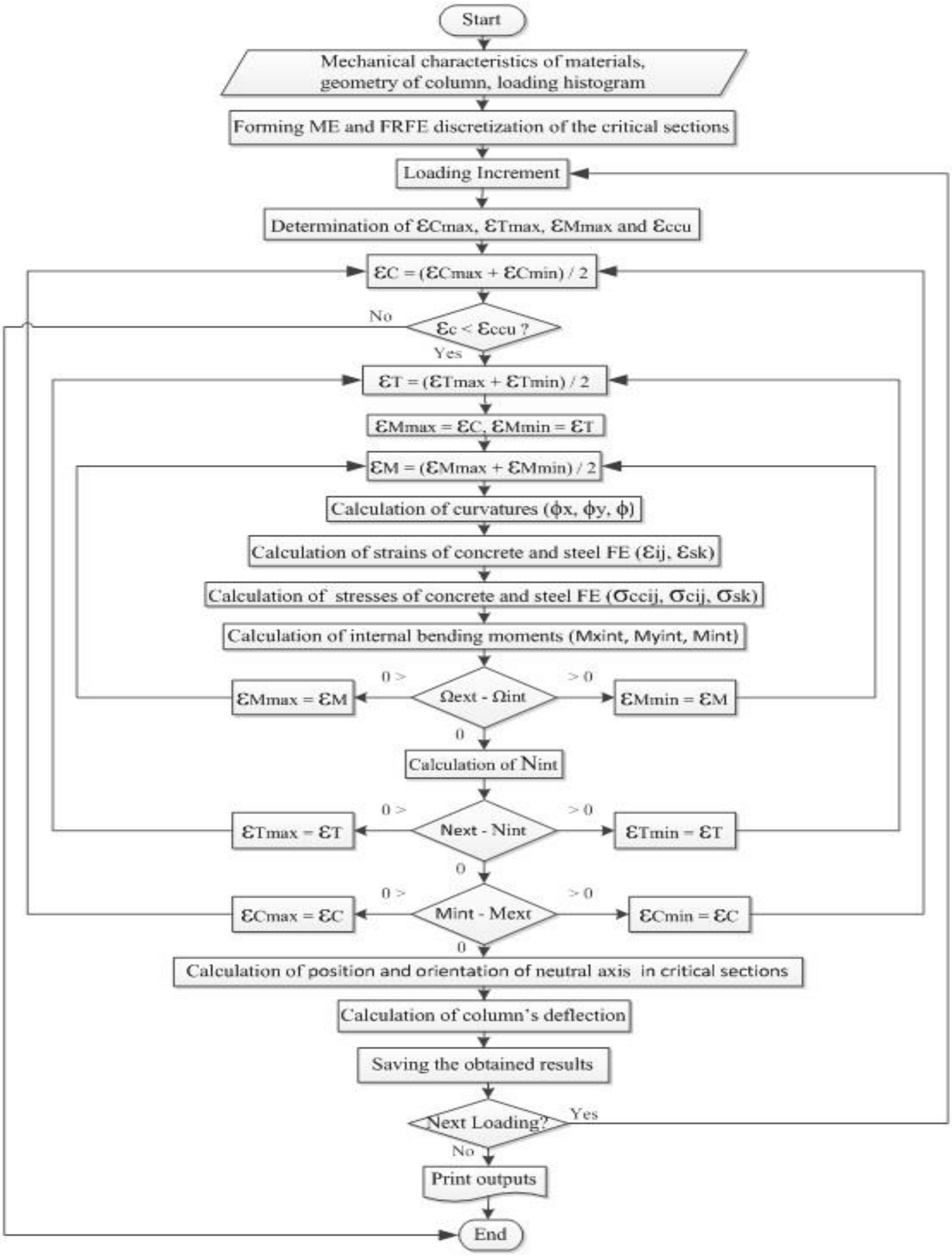

Fig. 7 Flow chart of the main parts of the simulation of columns under OPFAL

$$\varepsilon_{Cmin} = \varepsilon_C \qquad \text{(for } M_{int} > M_{ext}\text{)} \tag{73}$$

$$\varepsilon_{Cmax} = \varepsilon_C \qquad \text{(for } M_{int} < M_{ext}\text{)} \tag{74}$$

In the next iteration $(i+1)^{th}$, the following equation is applied

$$\varepsilon_{C(i+1)} = (\varepsilon_{Cmin(i)} + \varepsilon_{Cmax(i)})/2 \tag{75}$$

By calculating the strains and stresses of concrete and steel FE, internal moments and orientation angles and axial forces, and verification of the equilibrium of external and internal efforts during a set of the successive iteration process, this should conform to the following equilibrium condition

$$M_{ext} = M_{int} \tag{76}$$

2.11 Convergence criteria

To achieve acceptable accuracy within a reasonable calculation time, the convergence tolerances are considered as

$$|\Omega_{ext} - \Omega_{int}| \leq 0.1° \tag{77}$$

$$|N_{ext} - N_{int}| \leq 0.001\,|N_{ext}| \tag{78}$$

$$|M_{ext} - M_{int}| \leq 0.001\,|M_{ext}| \tag{79}$$

2.12 Calculation of deflections

In the proposed simulation an Elasto-Plastic Method (EPM) proposed by Priestley and Park (1987) is used. This method is based on the evidence that a column is highly affected in the critical zone when a lateral load is applied. Immediately following the peak value of the *M*-ϕ curve of the critical section, a very important local effect occurs at the critical section where a pseudo plastic hinge appears. Once the peak has passed, curvature enhancement is concentrated in the critical zone. While in the other regions, the curvatures decrease rapidly to near zero.

When applying EPM to calculate deflections, Eqs. (80) and (81) are used

$$\delta = \left(\frac{\phi}{3}\,L^2\right) \qquad \text{(for } \phi \leq \phi_p\text{)} \tag{80}$$

$$\delta = \left(\frac{\phi_p}{3}\,L^2\right) + (\phi - \phi_p)(L_p)(L - 0.5\,L_p) \qquad \text{(for } \phi \geq \phi_p\text{)} \tag{81}$$

Where δ represents the deflection at the top of ME (half column); ϕ represents the curvature at critical section and ϕ_p represents its value at the plastic hinge performance phase, respectively; L and L_p represent the lengths of ME and the length of plastic hinge, respectively.

There is a good agreement between simulated deflections by applying the mentioned method and the experimental results.

3. Developed computer program

A computer program entitled Column Non-Linear Analysis Program (CNLAP) has been developed by the authors to simulate numerically the behavior of RC columns under OPFAL and COLFAL in any direction (i.e., BBMAL applied on sections), considering the nonlinear behavior of materials. CNLAP has some sub-programs such as:

- BBCS (Biaxial Bending Column Simulation) which simulate the behavior of ME under COLFAL and considers FRFE in discretization of the sections,
- OPA (Oriented Pushover Analysis) which simulate the behavior of ME under OPFAL and considers VOFE in discretization of sections,
- CCS (Confined Concrete Simulation),
- UCS (Unconfined Concrete Simulation),
- SBS (Steel Bars Simulation),
- NAPS (Neutral Axis Position Simulation),
- DC (Deflection Calculation) and
- DIC (Damage Index Calculation).

In CNLAP, the two options for discretization of sections are applied: in BBCS sections are discretized into FRFE and in SOPA, the sections are discretized into VOFE. CNLAP takes into account the confining effect of the transverse reinforcement and simulates the loss of the concrete cover. It allows the determination of the failure, the internal local behavior of critical sections (i.e. strains, stresses, neutral axis position, cracks positions, loss of material, microscopic damage index, etc.) and the external global behavior of the column (curvature, deflection, rigidity, damping ratio, macroscopic damage index (Sadeghi 2011), etc.).

4. Experimental data and reference column

The proposed numerical simulation has mainly been validated by the experimental test results of Garcia Gonzalez performed on the full-scale columns under COLFAL and OPFAL (Garcia Gonzalez (1990), Sieffert *et al*. (1990)) and the experimental tests/simulation of Park (1972).

The dimensions and characteristics of the columns tested by Garcia Gonzalez are as follows: rectangular section 18 cm×25 cm, height of 1.75 m, four longitudinal reinforcement with a diameter of 12 mm (ϕ12), concrete of strength of 42 MPa, stirrup ties of diameter 6 mm with a longitudinal spacing of 9 cm, yielding stress of steel bars: 470 MPa. This column is fixed at the bottom, free at the top and is under an axial force of 500 kN and OPAL or COLFAL at the top. The horizontal loads through different orientations Ω have been applied on the top of the columns. In this paper, Garcia Gonzalez's Column is called "reference column" and its section is called "reference section".

5. Some simulation results

Comparisons of numerically simulated results using the proposed simulation algorithm and experimental tests on full-scale RC members are reflected in Figs. 8 to 13. The comparison indicates a close agreement between the proposed simulation and the experimental test results.

In Fig. 8, the results of the proposed simulation using FRFE and experimental test/simulation of

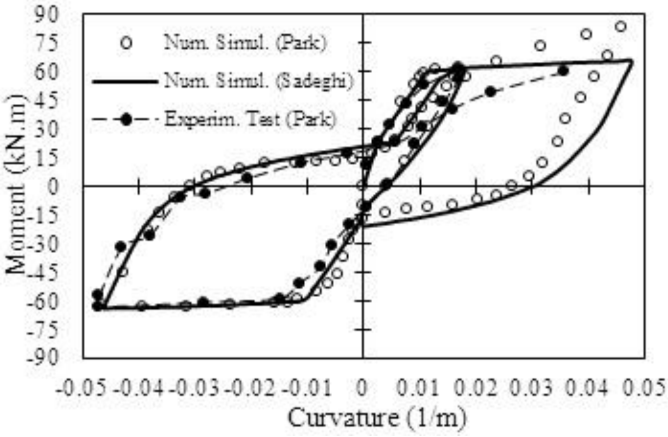

Fig. 8 Comparison of proposed simulation and experimental test/simulation of Park

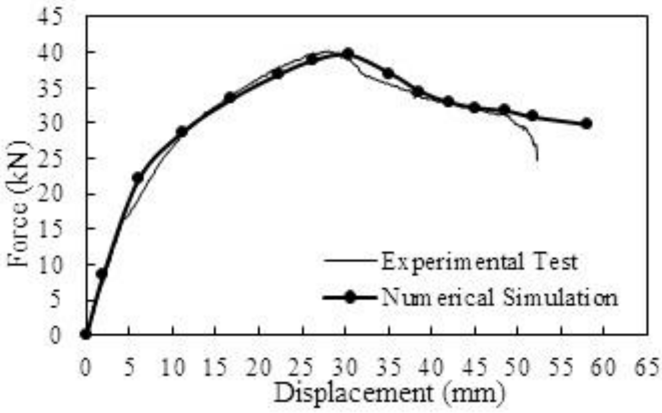

Fig. 9 Comparison of the proposed simulation and experimental tests results, $\Omega = 0^{\circ}$

Park for a CL case are compared. As this figure shows there is good agreement between simulated and experimental results.

In Fig. 9, the results of the proposed simulation are compared with experimental test results (Garcia Gonzalez 1990) on the reference columns under OPFAL with the orientation of $\Omega = 0°$. For this force orientation angle using FRFE or VOFE discretization options gives the same results.

In Fig. 10, the results of the proposed simulation using VOFE and FRFE are compared with experimental test results for OPFAL case with the orientation of $\Omega = 45°$. As this figure shows for loading up to 85% of the ultimate strength of the section there is a better agreement between simulated results using VOFE discretization and experimental results than when the FRFE discretization model is employed.

Fig. 11 shows the variations of the position of the neutral axis at the critical section of the reference column when the pushover force with the orientation of $\Omega = 45°$ is increased to its maximum value. As shown in this figure, by increasing the pushover force (or moment), the neutral axis moves from outside the section to point T with an inclination of about $\alpha = 55°$ and

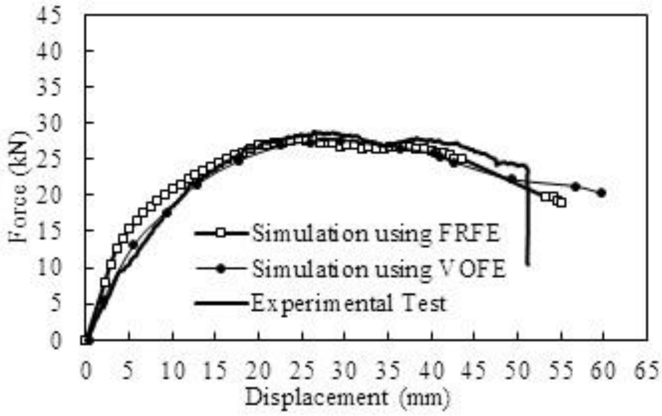

Fig. 10 Comparison of experimental test and simulations using VOFE and FRFE, Ω = 45°

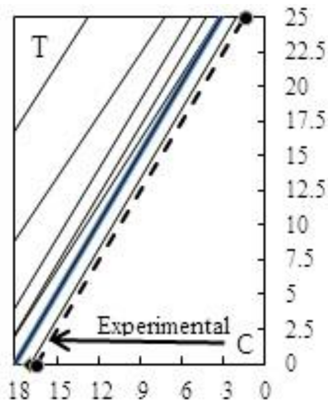

Fig. 11 The neutral axis positions of the reference section, Ω = 45°

then shifts toward the center of the section when the maximum load is applied with an inclination of α = 60°.

When the load is increased, the neutral axis moves with an approximately constant inclination up to the ultimate strength of the section. The results of measurements on the full-scale experimental tests (Garcia Gonzalez 1990), for the neutral axis position when peak load is applied on the critical section of the reference column is shown by the dashed lines in Fig. 11. Experimental test results showed an inclination of α = 59° for the neutral axis when peak load was applied on the section for an orientation of Ω = 45°. As Fig. 11 shows, there is a good agreement between simulated values and experimental results.

Figs. 12 and 13 compare the simulated values and experimental test results (Garcia Gonzalez 1990) of average rigidity and equivalent viscous damping ratio for COLFAL.

Fig. 14 shows the variations of the M-ϕ curves of the critical section of the reference column under OPFAL for different values of axial force "Next" for the pushover orientation of Ω = 30°. As this figure indicates, the rigidity and ultimate strength of the column are increased by increasing the axial force. Also, it shows that the failure of the column occurs earlier by increasing the axial force, meaning a heavy axial load makes the column fragile, imposing a big loss of

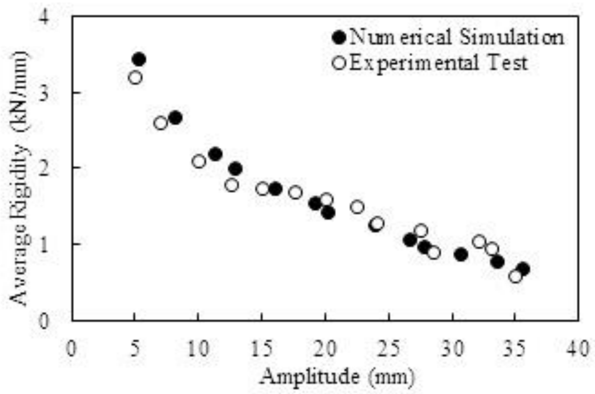

Fig. 12 Comparison of simulated and tested average rigidities, COLFAL, Ω = 30˚

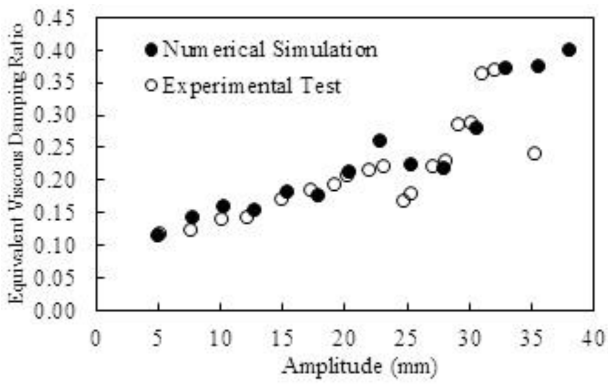

Fig. 13 Comparison of simulated and tested equivalent viscous damping ratios, COLFAL, Ω = 30˚

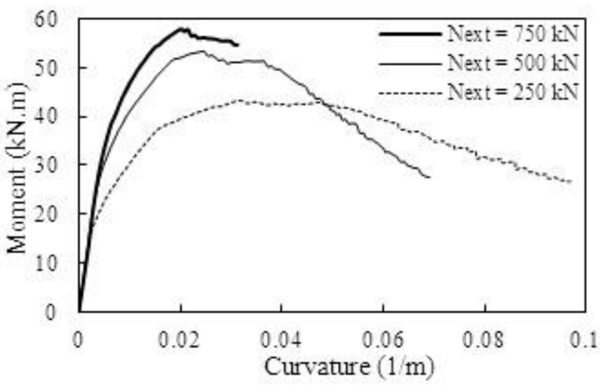

Fig. 14 Effect of axial force on the response of the critical section, Ω = 30°

material and reducing the ductility of the column. This type of fragility, reduction of ductility and loss of material needs to be carefully considered in prestress structural members design. Similarly, care needs to be taken in the design of structures being designed for seismic zones having a significant vertical force component of earthquake loading.

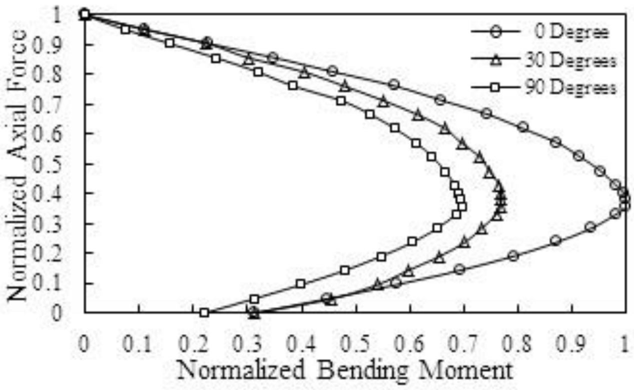

Fig. 15 Interaction diagram of reference section under different applied lateral force orientations

Fig. 15 presents the axial force-moment interaction diagram of the reference section under different applied lateral force orientations.

6. Conclusions

A nonlinear numerical simulation algorithm using FRFE or VOFE has been proposed to simulate the behavior of RC columns subjected to COLFAL or OPFAL (BBMAL on sections) together with a FE computer program entitled CNLAP. The proposed simulation is applicable to RC columns subjected to CL or ML. The proposed nonlinear numerical solution has been validated by experimental data obtained in laboratory tests.

When the column is subjected to ML or OPFAL, the critical sections are discretized into VOFE which always stay parallel to the neutral axis. To minimize the number of elements, two different widths are adopted for VOFE in a section. By using this type of VOFE discretization, the time of calculation is significantly slightly decreased, and since VOFE always stay parallel to the neutral axis, variations of stress distribution along the element is significantly decreased. Therefore, the proposed method using VOFE presents more accurate results and is slightly faster compared to the method using FRFE.

Acknowledgements

The financial and technical support of University of Nantes/Ecole Central de Nantes and Girne American University are appreciated.

References

Alnoury, S.I. and Chen, W.F. (1982), “Behavior and design of reinforced and composite concrete sections”, *J. Struct. Div.*, ASCE, **108**(6), 1266-1284.

Amziane, S. and Dubé, J.F. (2008), “Global RC structural damage index based on the assessment of local

material damage”, *J. Adv. Concrete Tech.*, **6** (3), 459-468.
Brondum-Nielsen, T. (1984), “Serviceability limit state analysis of concrete sections under biaxial bending, *J. ACI*, **81**(5), 587-593.
CEB Code (1978), Code-Modéle CEB-FIP pour les structures en béton, Bulletin d’information no. 124-125F, Comité Euro-International du Béton, Vol. 1-2, Paris, France.
Dundar, C. and Tokgoz, S. (2012), “Strength of biaxially loaded high strength reinforced concrete columns”, *Struct. Eng. Mech.*, **44**(5), 649-661.
Garcia Gonzalez, J.J. (1990), “Contribution á l’étude des poteaux en béton armé soumis á un cisaillement dévié alterné”, Ph.D. Dissertation, University of Nantes/Ecole Central de Nantes, Nantes.
Hsu, C.T. and Mirza, S. (1973), “Structural concrete biaxial bending and compression”, *J. Struct. Div.*, ASCE, **99**(ST2), 2317-2335.
Massumi, A., Monavari, B. (2013), “Energy based procedure to obtain target displacement of reinforced concrete structures”, *Struct. Eng. Mech.*, **48**(5), 681-695.
Park, R., Kent, D.C. and Sampson, R.A. (1972), “Reinforced concrete members with cyclic loading”, *J. Struct. Div.*, ASCE, **98**(ST7), 1341-1359.
Priestley, M.J.N. and Park, R. (1987), “Strength and durability of concrete bridge columns under seismic loading”, *ACI Struct. J.*, **84**(1), 61-76.
Richard Yen, J.Y. (1991), “Quasi-Newton method for reinforced concrete column analysis and design”, *J. Struct. Div.*, ASCE, **117**(3), 657-666.
Rofooei, F.R., Mirjalili, M.R. and Attari, N.K.A. (2011), “Spectra combination method for pushover analysis of special steel moment resisting frames”, *Int. J. Civil Eng.*, **10**(4), 245-252.
Sadeghi, K. (1995), “Simulation numérique du comportement de poteaux en béton arme sous cisaillement dévié alterne”, Ph.D. Dissertation, University of Nantes/Ecole Central de Nantes, Nantes.
Sadeghi, K. (2001), “Numerical simulation and experimental test of compression confined and unconfined concrete”, Technical Report Submitted to Water Resources Management Organization, Ministry of Energy, Concrete Laboratory of Power and Water University of Technology, Tehran, Iran.
Sadeghi, K. (2011), “Energy based structural damage index based on nonlinear numerical simulation of structures subjected to oriented lateral cyclic loading”, *Int. J. Civil Eng.*, **9**(3), 155-164.
Sadeghi, K. (2014)., “Analytical stress-strain model and damage Index for confined and unconfined concretes to simulate RC structures under cyclic loading”, *Int. J. Civil Eng.*, **12**(3), 333-343.
Sheikh, S.A. (1982), “A comparative study of confinement models”, *ACI J.*, ***79***(4), 296-305.
Sieffert, J.G., Lamirault, J. and Garcia, J.J. (1990), “Behavior of R/C columns under static compression and lateral cyclic displacement applied out of symmetrical planes”, *Proceedings of the 1st European Conference on Structural Dynamics (EUROPEAN 90)*, **1**, Bochum, June.
Tabsh, S.W. (2013), “Comparison between reinforced concrete designs based on the ACI 318 and BS 8110 codes”, *Struct. Eng. Mech.*, **48**(4), 467-477.
Yau, C.Y., Chan, S.L. and So, A.K.W. (1993), “Biaxial bending of arbitrarily shaped reinforced concrete columns of arbitrary shape”, *Struct. J. ACI*, **90**(3), 269-273.
Zak, L. (1993), “Computer analysis of reinforced concrete sections under biaxial bending and longitudinal load”, *Struct. J. ACI*, **90**(2), 163-169.

CC